Research Article Vol. 33, No. 20 / 6 Oct 2025 / Optics Express 42829
Optics EXPRESS

O-band quantum-dot mode-locked laser frequency comb for terabit optical transport

LAKSHMI NARAYANAN VENKATASUBRAMANI,[1,†,*] AHMED GALIB REZA,[1,†] SEAN O'DUILL,[1] MIKHAIL BUYALO,[2] JANINA RAUTERT,[2] ALEXEY GUBENKO,[2] AND LIAM BARRY[1]

[1]School of Electronic Engineering, Dublin City University, Dublin 09, Ireland
[2]Innolume, Konrad-Adenauer-Allee 11, 44263 Dortmund, Germany
[†]These authors contributed equally to this work
[*]lakshminarayanan.venkatasubramani@dcu.ie

Abstract: High-capacity data transmission for intra- and inter-data center links is essential to handle the massive increase in data traffic. To address the insatiable demands, IEEE has been working on creating specifications for 800 GbE (IEEE 802.3df) and 1.6 TbE (802.3dj) using a multi-lane distribution method by aggregating 100 Gbps and beyond lanes. Optical frequency comb sources based on semiconductor mode-locked laser (MLL) are cost- and energy-efficient optical sources that can enable multi-lane transmission systems. Here, we demonstrate 14×100 Gbps PAM4 signals and 10×100 Gbps probabilistically shaped PAM8 signals over 10 km SMF with an O-band InAs/InGaAs quantum dot mode-locked laser (QD-MLL) consuming only ~284 fJ/bit. We also successfully demonstrated 128 Gbps/λ OOK signal transmission with four lines from the QD-MLL spaced at 160 GHz, with a single booster amplifier for multichannel amplification. We show that the performance of the ≥1 Tbps and 512 Gbps WDM signals is within the standard FEC limits with preamplifier and booster semiconductor optical amplifiers, respectively.

1. Introduction

Data storage and transport in data centre (DC) networks have become enablers for many cloud and web-based applications. Increasing demand for high-speed data transmission in both wireline and wireless networks and the proliferation of computation and resource-intensive technologies have led to a substantial rise in the number of DCs and exponential bandwidth requirements within each DC. The DC network topology can be categorised as intra-, campus-, or inter/metro-DC interconnects (DCI) for transmission distances up to 2 km, 10 km, and 80 km, respectively. Closely located data centres are interconnected with a campus-DCI network to form a larger logical DC unit. Hence, campus-DCI links require larger bandwidth and lower latency transmission than metro-DCI links [1]. In each fibre link, deploying parallel spectral channels and employing multiple signalling levels at a higher symbol rate in each channel can accommodate the growing demands for high-capacity short-reach systems.

High symbol rate intensity-modulated direct detection (IM/DD) systems are best suited for short-reach DCI links due to their lower digital signal processing (DSP) complexity, better energy and cost efficiency, and support of backward compatibility relative to coherent systems. The O-band operating systems, centred around 1.3 μm, present advantages compared to 1.5 μm centred systems since they offer ultra-low dispersion and are thus robust against frequency-selective power fading, especially in large-bandwidth systems. Optical carriers for wavelength division multiplexed (WDM) data transmission can be derived from independent laser modules or from a single optical frequency comb source [2]. Employing multiple laser sources will increase the

#569003 https://doi.org/10.1364/OE.569003
Journal © 2025 Received 27 May 2025; revised 18 Sep 2025; accepted 18 Sep 2025; published 30 Sep 2025

Optics EXPRESS

system's cost and power requirements [3]. In contrast, multi-wavelength optical comb sources allow for dense photonic integration and can be more advantageous from a practical and economic perspective.

Semiconductor mode-locked lasers (MLLs) are efficient on-chip WDM sources, offering a smaller footprint and high-power efficiency. Recently, many demonstrations have been made with quantum dot MLLs (QD-MLL) as O-band optical frequency comb sources owing to their reasonable power per channel [4–9], indicating an excellent potential for future short-reach high-capacity systems. Aggregated power loss from fibre attenuation, splitting/filtering, and switching can limit the transmission performance of campus DCI links that employ comb sources, introducing the requirement for optical amplifiers [10]. Semiconductor optical amplifiers (SOA) are favourable due to their small footprint, reduced energy consumption, and the ability for photonic integration [11,12]. In this manuscript, we focus primarily on the detailed characterisation of the two-section Fabry-Perot QD-MLL and its potential to support multi-lane terabit transmission in conjunction with the use of SOA to achieve the required power budgets for system performance.

Previously, we demonstrated 100 Gbps single channel transmission over 10 km standard single mode fibre (SMF) using InAs/InGaAs quantum dots in GaAs/AlGaAs material-based QD-MLL [5] with booster SOA and DWDM transmission with a SOA preamplifier [13]. This work extends our previous work to perform a detailed noise analysis of QD-MLL and demonstrate $\geq$ Tbps transmission with 10 and 14 channels with 100 Gbps per-channel capacity. In scenarios with low-bandwidth component availability, employing a modulation with higher cardinality is an effective strategy to maintain the desired transmission rate. Scaling the cardinality of PAM (like PAM8) requires more considerable optical power per channel and lower intensity noise that is within the standard performance limits. The mode partition noise from the MLL may limit scaling beyond PAM4, though we optimise the entropy of the PAM8 by employing probabilistic constellation shaping (PS) to achieve the same 100 Gbps per-channel capacity. Data transmission needs to be reconfigured based on instantaneous demand or depending on the system complexity requirements. The QD-MLL lines can be effectively adjusted using an optical processor or switch, which allows for the precise selection of lines at the desired frequency spacing. Using 128 Gbps per channel On-Off keying signal, we demonstrate this as a proof-of-concept experiment by selecting four comb lines spaced at 160 GHz from the QD-MLL. In this experiment, we employ a single quantum-dot SOA as a booster amplifier to compensate for the filtering and modulation losses. Employing a single SOA for high-capacity intra-DCI links based on WDM technology can dramatically reduce power consumption per transmitted bit.

For transmission lengths greater than intra-DCI distances, higher optical fibre launch powers are preferred in DWDM systems to satisfy the receiver sensitivity requirement. However, performance can be affected due to interchannel fibre nonlinearities in a typical DWDM transmission system, such as four-wave mixing and cross-phase modulation, whose impairments of optical signals are significantly worse due to the low dispersion in the O-band [14]. In this work (employing PAM modulation), we also demonstrate the use of an SOA as a preamplified receiver, which enables lower fibre launch powers and, hence, lessens the impact of the fibre nonlinearities. Higher-order modulation formats such as PAM8 are prone to distortions due to SOA nonlinearity, and probabilistic shaping helps alleviate these distortions. The presented results demonstrate the potential development of a compact small form factor module for next-generation 800 GbE or 1.2/1.6 TbE campus-DCI links based on 1.3 μm multi-channel technology when employed with a silicon photonic-integrated optical frequency comb modulator [8,15–17] and SOAs. The presented results using the optical frequency comb and SOA show the working capability of the devices and are envisaged to be used in a transmitter assembly as shown in Fig. 1. Several demonstrations of quantum dots grown directly on CMOS-compatible Si substrates pave the way to realise the envisaged transmitter assembly [18,19]. The use of a single SOA for amplification

Optics EXPRESS

of the WDM signal can ensure the power budget required for higher capacity and longer link lengths is met with reduced energy per bit. This type of system architecture can also be combined with an SOA preamplified receiver to further enhance data rate and/or interconnect reach.

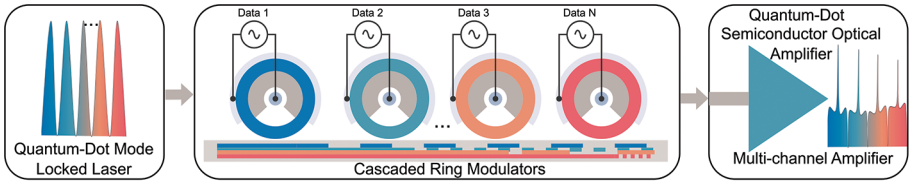

Fig. 1. Descriptive cartoon of the envisaged transmitter assembly incorporating the quantum-dot mode-locked laser, resonant ring modulators and a single semiconductor amplifier for amplifying multiple channels simultaneously.

2. QD-MLL characterisation

The optical frequency comb is based on an InAs/InGaAs quantum-dot passively mode-locked laser operating in the O-band, centred around 1310 nm. The structure consists of a two-section device that includes a gain section and a saturable absorber section. Figure 2 presents the schematic diagram of the mode-locked laser and its corresponding epitaxial structure of the device. Molecular beam epitaxy (MBE) is employed as the growth method in the manufacturing of the device. The active layer has ten quantum-dot layers in GaAs waveguide between AlGaAs claddings. A 99% high-reflectivity coating is applied to the absorber end of the cleaved Fabry-Perot laser, while a 30% reflection coating is applied at the opposite end to facilitate laser output from one side. Isolation between the p-contacts of the laser diode and absorber section is achieved by a trench, which is etched into the structure. A standard 14-pin butterfly package houses the O-band QD-MLL source with a free spectral range (FSR, $\Delta\nu$) of about 80 GHz. The FSR is mainly determined by the length of the cavity (L) and calculated as $\Delta\nu = \frac{c}{2n_g L}$, where c is the speed of light in vacuum and n_g is the group index of the gain material. For this QD-MLL, the cavity length is about 500 μm and the absorber length is about 75 μm. By properly designing the cavity length, it is possible to achieve a spacing in the range of 25 to 100 GHz [20].

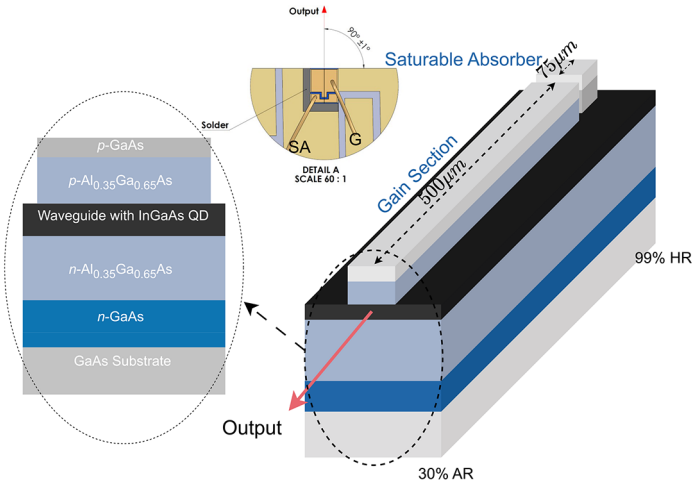

Fig. 2. Schematic diagram of the two-section quantum-dot mode-locked laser and its corresponding epitaxial structure of the device.

Optics EXPRESS

2.1. Spectral characterisation

Figure 3 shows the schematic of the experimental setup to characterise the optical spectrum, intensity noise, and phase noise of the QD-MLL. We first tuned the injection bias current from 0 mA to 220 mA at discrete temperatures in the range from $20^{\circ}C$ to $60^{\circ}C$ to observe the device's light-current (L-I) characteristics. In all of the experiments, we have operated the saturable absorber (SA) at a zero bias voltage. Although an increase in the saturable absorber voltage can increase the number of lines, this will result in a reduced power and carrier-to-noise ratio of the generated lines [9]. Hence, we work with a SA bias of 0 volts. Figure 4(a) shows the measured output power as a function of the bias current and at various temperatures. The threshold for lasing is measured at around 18 mA, 20 mA, and 30 mA bias currents at $25^{\circ}C$, $40^{\circ}C$ and $60^{\circ}C$, respectively. Figure 4(b) shows the temperature-dependent laser diode voltage as a function of the bias current. We next tuned the injection bias current from 100 mA to 180 mA and observed the optical spectrum using an optical spectrum analyser (OSA) with a resolution bandwidth (RBW) of 0.01 nm.

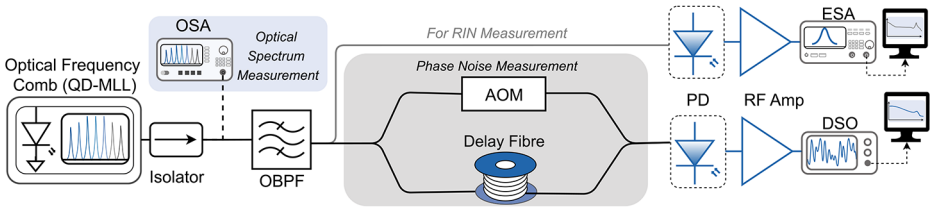

Fig. 3. Schematic of the experimental setup for optical spectrum, RIN and phase noise measurements of the optical lines from the QD-MLL comb.

Figure 5(a) shows the optical spectrum of the QD-MLL at various bias currents, and we can observe that the spectrum is tunable over >10 nm by changing the bias current. Figure 5(b) shows the number of lines at various bias currents and within 2 dB to 10 dB of flatness. We can observe at least ten lines within the 4 dB flatness for bias currents exceeding 100 mA. For further analysis and data transmission demonstration, we consider an operating bias current of 140 mA as an optimum value to get a wider comb centred around 1310 nm (about 14 lines) and have sufficient optical power per comb line to be within 6 dB flatness. We then fixed the bias current at 140 mA and tuned the operating temperature from 20°C to 60°C as shown in Fig. 5(c). The inset of Fig. 5(c) shows the central wavelength (λ_c, measured within 10 dB flatness) drift for the temperature tuning. From the mean slope of this curve, we estimate that the tuning coefficient of this laser is about 0.7 nm/°C. Figure 5 (d) shows the number of lines within a certain degree of flatness when the device is tuned at various temperatures. We can observe that the overall QD-MLL spectrum is tunable over >25 nm with changing temperatures, and presents stable operation, even at higher temperatures, making it suitable for DCI.

In the mode-locking regime, the mode-partition noise is low, resulting in a strong narrowing of the beating linewidth. On the contrary, as for conventional Fabry-Perot lasers, the lines are not locked, and the mode-partition noise is high, so the beating linewidth is degraded. Therefore, we study the beating of the modes and look at the RF beatwidth. We have recorded operating points from 20 to 60 °C, from 150 to 200 mA with a 25 mA step. Generally, at 60°C and at currents of 175mA and higher, we do not observe mode-locking (or the signal was too weak to see it). In all the cases, we measured the beat width less than 500 kHz at -20 dB level, together with the absence of the side peaks, which stands as evidence for stable mode-locking. These measurements were done after applying two cascade frequency down conversions to be in the bandwidth of our detection system, with an amplifier in between the modulators.

Optics EXPRESS

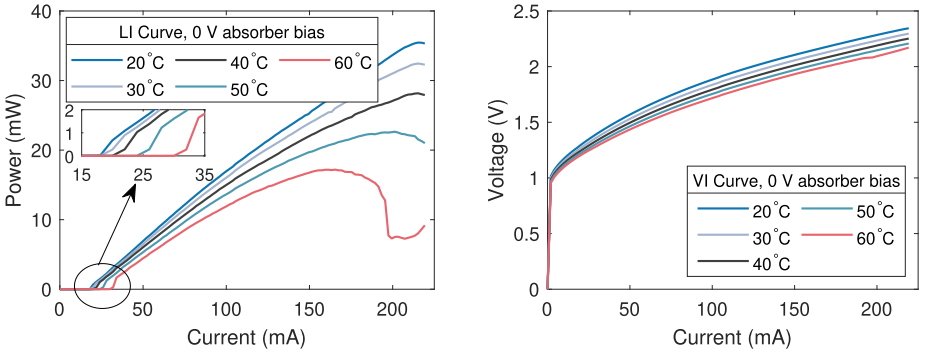

Fig. 4. (a) L-I and (b) V-I characteristics of the QD-MLL, operated at various bias currents and at different temperatures.

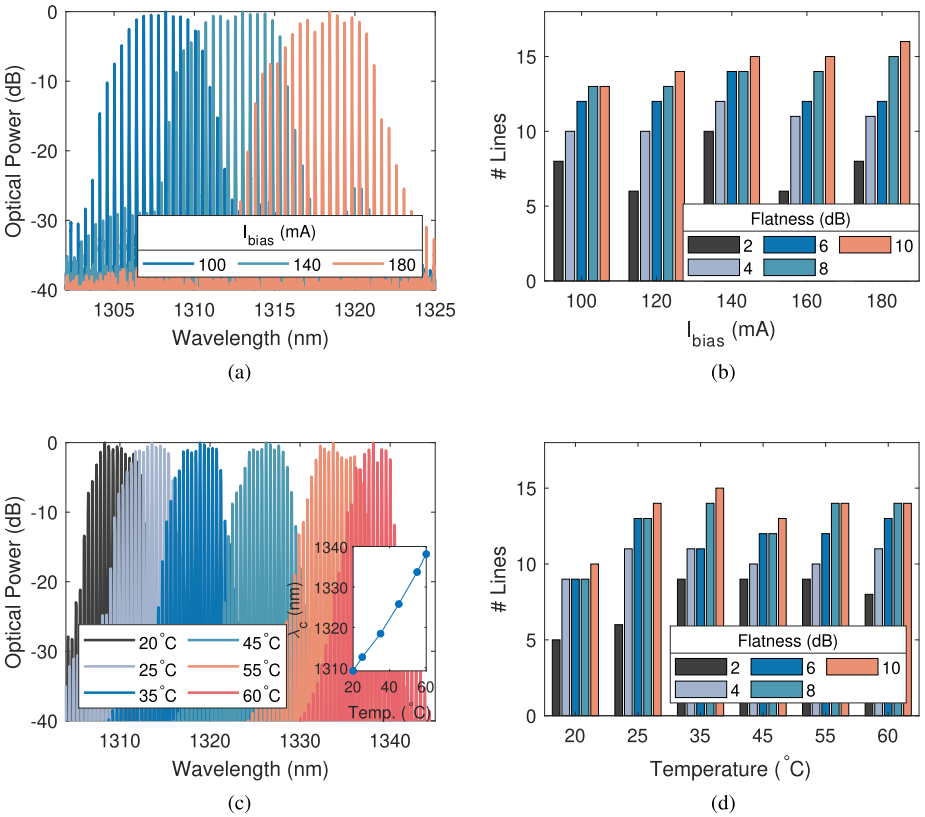

Fig. 5. (a) Overlapped optical spectra of the QD-MLL lines at various bias currents and at 25°C, (b) Number of lines under varied bias current within specific flatness levels, (c) Overlapped lasing modes of QD-MLL operated at 140 mA bias current and tuned to operate at different temperatures (inset shows the mean wavelength drift as function of temperature) and (d) Number of lines under temperature variation within specific flatness levels.

Optics EXPRESS

2.2. Intensity noise measurments

We proceed to characterise the QD-MLL's relative intensity noise (RIN) and phase noise for selected lines with the schematic of the measurement setup as shown in Fig. 3. We operate the QD-MLL at 140 mA bias current for the experiments and maintain the operating temperature at 24.5°C. We filter out the lines of interest from the QD-MLL to measure the RIN using an optical bandpass filter (OBPF). We then detect the optical signal using a 30 GHz bandwidth photodetector (PD). The detected signal is then amplified using a 50 GHz RF amplifier and is fed to the electrical spectrum analyser (ESA, RS FSW50). The electrical spectrum and information on the shot and thermal noise are then used to compute the RIN as shown in Fig. 6 [21]. A low integrated RIN value of -165 dB/Hz is obtained from 1 MHz to 10 GHz for the whole QD-MLL comb spectrum. Filtered lines exhibit an additional RIN in the low-frequency range of 1 MHz to 100 MHz, as shown in Fig. 6 due to mode partition noise (MPN). The RIN of the filtered lines presents a level below -145 dB/Hz beyond 600 MHz, demonstrating the potential to support higher-cardinality PAM transmission systems.

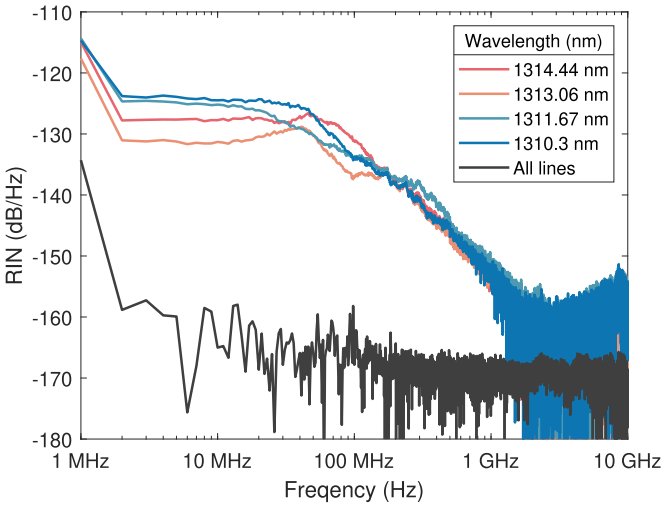

Fig. 6. Relative intensity noise of the whole O-band QD-MLL spectrum and at certain filtered individual wavelength channels of QD-MLL.

2.3. Phase noise measurments

The frequency modulation noise (FM-noise) of each of the lasing modes is measured, and Fig. 7 shows the spectral density of FM-noise power at various frequency offsets. This is done as follows: the OBPF is tuned to select each mode individually, which is then sent to the phase noise measurement system based on the self-delayed heterodyne method [22]. Each curve has been multiplied by 2π so that horizontal portions of the curves can be interpreted as Lorentzian linewidths [23]. The filtered light from the MLL is frequency-shifted by 200 MHz using an acousto-optic modulator (AOM). Hence, the maximum frequency range that the technique can measure is limited to 200 MHz. The modes are labelled L1 (1308.99 nm) for the mode with the smallest wavelength in the MLL comb spectrum and L13 (1314.97 nm) for the mode with the longest wavelength in the comb spectrum.

We note three distinct regions of FM-noise in the curves: at the lowest frequencies (<1 MHz), we observe typical '1/f' style FM-noise arising from slow wavelength drift of the lasing mode due to technical and environmental noise that is mainly associated with the drive current to the laser; in the middle-frequency range, we observe what appears to be FM-noise arising from slow

Optics EXPRESS

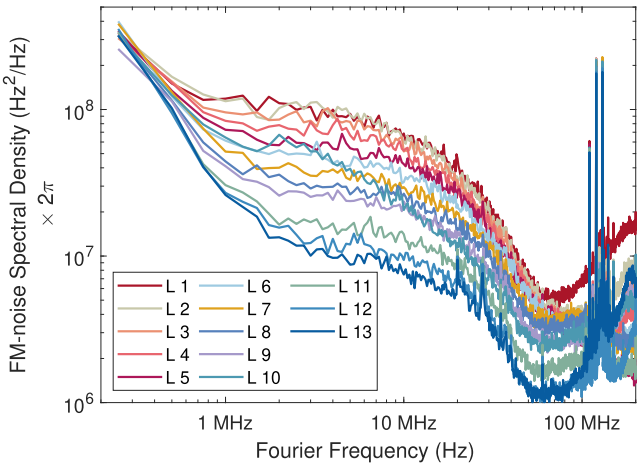

Fig. 7. FM-noise power spectral density (PSD) measurements of filtered individual wavelengths of the QD-MLL when operated at 140 mA bias currents. Each of the PSD curves has been scaled by 2π.

timing jitter that rolls off after 10 MHz; and the intrinsic linewidth of the modes, interpreted by the flat FM-noise in this spectral region, in the frequency region above 50 MHz. The increase in the FM noise occurring around 100 MHz is due to noise in the measurement system, including contributions from photodetectors, RF amplifiers, and analogue-to-digital converters.

Firstly, we analyse the intrinsic linewidth portions of the FM-noise curve. The FM-noise value of each mode at the frequency of 50 MHz is plotted in Fig. 8(a). The plot shows a quadratic dependence with respect to the mode index number. We note that the quadratic dependence for linewidth (and FM-noise) on the mode index number is related to the timing jitter experienced by the pulses as they traverse the mode-locked laser cavity [24]. We fit the intrinsic FM-noise according to the modal dependence on linewidth caused by spontaneous emission to the pulse timing jitter [24]

$$\Delta f(n) = B_0 + B_{RF}(n-13)^2, \tag{1}$$

with n in the range from [1,13]. B_0 is the linewidth of the mode with the lowest linewidth whose modal index is referenced to 1. While in principle, the '0' mode is in the centre of the spectrum for MLLs [24], for quantum dot MLLs, the mode with the smallest linewidth is typically found at the edge of the lasing spectrum; in this work we also find the mode with the smallest linewidth to be at the longest wavelength in the MLL spectrum at mode 13 in this case. The value of B_0 is 1.28 MHz, and the extracted value of RF linewidth, B_{RF} is 32 kHz. The RF linewidth is the linewidth of the beat signal from adjacent comb lines and gives an indication of the level of phase correlation between the comb lines.

Now, we analyse the FM-noise of the curves in the lower frequency part of the FM-noise spectrum from 1 MHz to 10 MHz. The FM-noise value at 5 MHz is plotted in Fig. 8(b) against the mode index number. The FM-noise resulting from this phenomenon is assumed to be caused by a contribution to the refractive index fluctuation from random free-carrier concentration in the wetting layer in the QD material. The FM-noise created by this process is independent of the cause of the intrinsic linewidth. Therefore, we subtract the intrinsic linewidth of each respective mode in order to calculate the FM-noise due to the free carriers in the wetting layer. Clearly, there is a quadratic dependence of FM-noise with respect to the mode index number, which indicates that there is a process within the laser cavity creating an additional timing jitter other than spontaneous emission that determines the intrinsic linewidth, the rolloff in this contribution

Optics EXPRESS

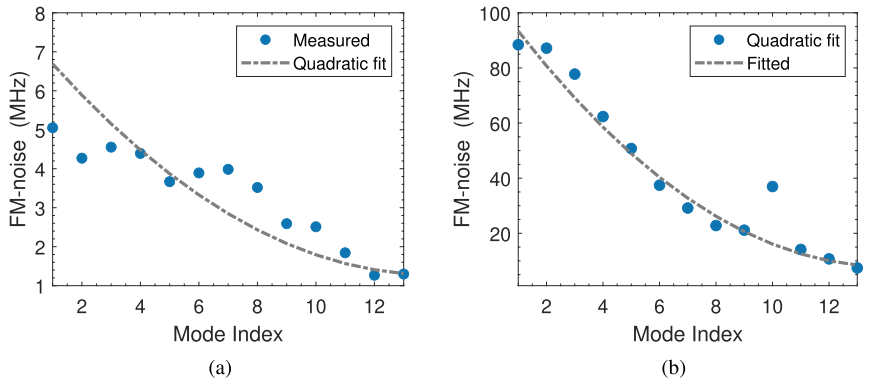

Fig. 8. (a) Extracted FM-noise value to indicate each filtered wavelength's intrinsic linewidth. (b) Extracted FM-noise at 5 MHz to show the dependence of the FM-noise arising from slow-speed jitter.

to the FM-noise after 10 MHz suggests that a slow-speed process causes the excess jitter. To analyse the excess frequency noise of a given mode, we take the data shown in Fig. 8(b) and fit to another quadratic curve

$$\Delta f_{ex} = B_{0,ex} + B_{RF,ex}(n - 13)^2 \tag{2}$$

We find that $B_{0,ex}$ is 8 MHz and $B_{RF,ex}$ is 505 kHz. The value of the line widths of the QD-MLL lines indicates their potential for coherent modulation transportation, especially at higher symbol transmission rates.

3. QD-MLL WDM transmission with SOA preamplifier

3.1. Experimental setup for PAM4 and PS-PAM8 transmission

We now demonstrate a system-level terabit per second transmission experiment (Fig. 9) with 14 lines of 50 GBd PAM4 and ten lines of 37.5 GBd PS-PAM8 employing the QD-MLL. We generate the 50 GBd PAM4 and 37.5 GBd PS-PAM8 signals offline. For probabilistic shaping, we generate the Maxwell-Boltzmann distribution-based PAM8 symbols [25] with entropies of 2.41, 2.676, 2.88 and 3 (corresponding to the uniform distribution (UD)) bits/symbol. The amplitude levels are pre-distorted to accommodate the nonlinear response of the external modulator. We then employ a 0.1 roll-off factor root-raised cosine (RRC) prototype filter to reduce the electrical bandwidth and load it in the 32 GHz arbitrary waveform generator (AWG). An RF amplifier (RF Amp 1, 23 dB gain) amplifies the analogue signal from the AWG. A 30 GHz O-band Mach-Zender modulator (MZM1) modulates all the lines of the QD-MLL with the amplified PAM4/PS-PAM8 electrical signal. Fig. 9 inset shows the optical spectrum of 15 modulated lines with indexing starting from L1 (line 1) and exhibits a 6 dB flatness over 14 lines (spectrum measured with a 20 dB attenuator before the OSA). The 80 GHz comb line spacing combined with the RRC pulse shaping of the signal ensures negligible interference between the channels. The generated 100 Gbps/λ PAM4/PS-PAM8 modulated data is transmitted over 10 km standard SMF with a ~4 dBm launch power. After the transmission, we filter each modulated line using a bandwidth-tunable optical bandpass filter (OBPF). The filtered modulated signal is then pre-amplified using a commercial quantum well SOA (QW-SOA), having a broader gain bandwidth of greater than 50 nm. Depending on the selected lines, the optical power of the filtered lines at the SOA input (150 mA bias current) varied from -8 to -14 dBm, with a corresponding gain ranging from 17.84 dB to 20.62 dB. Fig. 16(a) in the Appendix shows the SOA gain and output power as a function of the input power. To study the performance at different received optical power (ROP), we use a

Optics EXPRESS

variable optical attenuator (VOA) before detection. This signal is then detected using a 30 GHz photodetector (PD). An RF amplifier (RF Amp 2) with a gain of 24 dB amplifies the detected photocurrent, and a 33 GHz real-time scope (RTS, 100 GS/s) digitises the signal.

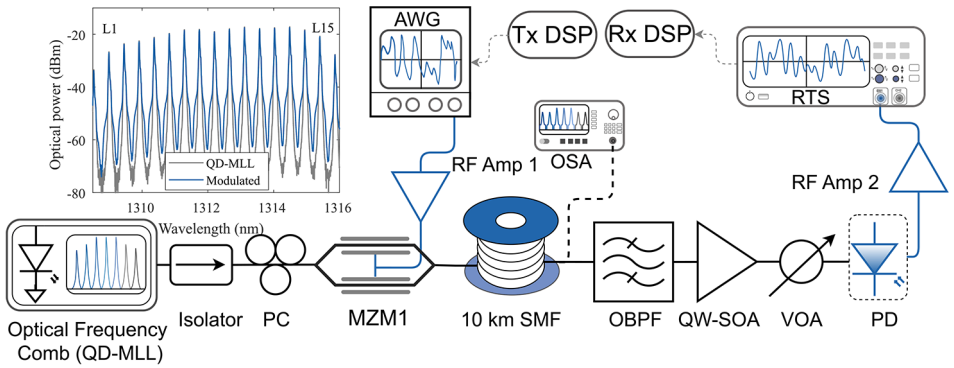

Fig. 9. Schematic of the experimental setup for the data transmission over 10 km standard single mode fibre employing the QD-MLL comb source and an SOA preamplifier. Inset shows the lines of QD-MLL before and after modulating with 50 GBd PAM4 signal.

3.2. Results

In the receiver-side offline DSP of the 100 Gbps signals, we first perform matched filtering with the RRC prototype filter and then resample the digitised signal from 100 GSamples/s to the symbol rate. We then employ a linear transversal feedforward equaliser (FFE) with 40 T-spaced taps. We use a larger tap size to reduce the effect of component-induced ISI due to their non-flat response in the desired bandwidth and for any residual dispersion compensation. Figure 10 shows the bit error ratio (BER) performance of the 10 km transmitted 1.4 Tbps PAM4 signals as a function of the channel wavelength at a fixed received optical power of -2 dBm. The performance of eleven 50 GBd PAM4 lines in the wavelength range of 1310.4 nm to 1314.9 nm, corresponding to a total data rate of 1.1 Tbps, attains a BER below the hard decision forward error correction (HD-FEC) limit of 3.8×10^{-3} with 7% overhead. The BER performance of all the PAM4 lines from 1309.9 nm to 1315.4 nm, constituting a total data rate of 1.4 Tbps, is under the soft decision FEC (SD-FEC) limit of 1.2×10^{-2} with 14.8% overhead [26]. The degraded performance in the outer channels is due to the lower input signal power to the SOA, translating to additional amplified spontaneous noise (ASE) in these channels.

We then evaluate the performance of the 10 km transmitted PS-PAM8 signals for the choice of entropy values for the 1310.11 nm wavelength channel at -2 dBm received optical power. Figure 10 top-left inset shows the measured BER as a function of signal entropy. We observe for an SOA preamplified receiver system, the UD-PAM8 (corresponding to an entropy value of 3 bits/symbol) signal could not reach the SD-FEC level BER performance due to mode partition noise from the QD-MLL and noise and distortions from SOA. Hence, we employ the PS-PAM8 signal with an entropy value of 2.676 bits/symbol as the best-fit choice for optimum performance and data rate. Figure 10 shows the BER performance of each filtered channel of the 37.5 GBd PS-PAM8 signals at 0 dBm received optical power. The performance of lines in the wavelength range of 1310.8 nm to 1314.9 nm (total 1 Tbps rate) attains a BER below the SD-FEC limit. Fig. 10 bottom-left inset shows the eye diagram of the processed PS-PAM8 signal, evaluated at -2 dBm received optical power after 10 km transmission. The clear eye-opening of the PS-PAM8 signal indicates a more considerable resilience to noise and SOA nonlinearity by the probabilistically shaped signals.

Optics EXPRESS

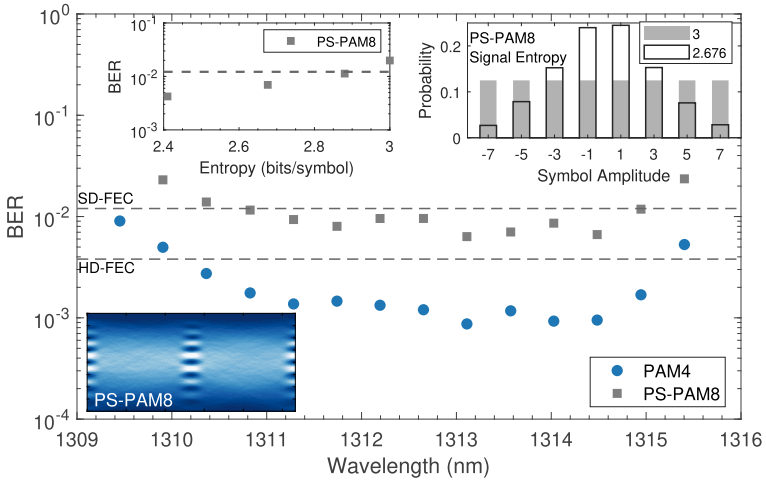

Fig. 10. BER performance of 50 GBd PAM4 (-2 dBm ROP) and 37.5 GBd PS-PAM8 (0 dBm ROP) signals after 10 km SMF as a function of wavelength. Insets- (top-left) BER performance for various entropies of the PS-PAM8 signal, (top-right) the probability distributions of uniform and 2.676 bits/symbol PAM8 signal, and (bottom-left) eye diagram of PS-PAM8 signal (1313.11 nm) at -2 dBm ROP.

Fig. 11 shows the BER performance of the 50 GBd PAM4 signals as a function of received optical power for selected line indices (the filtered channel spectrum is shown inset), and the performance falls within the SD-FEC limit for received optical powers >-7.5 dBm. Figure 11 inset shows the eye diagram and BER of the signal transmitted at the wavelength of 1311.11 nm and processed at a received optical power of -2 dBm with and without feedforward equaliser, clearly demonstrating the need for the FFE to improve system performance.

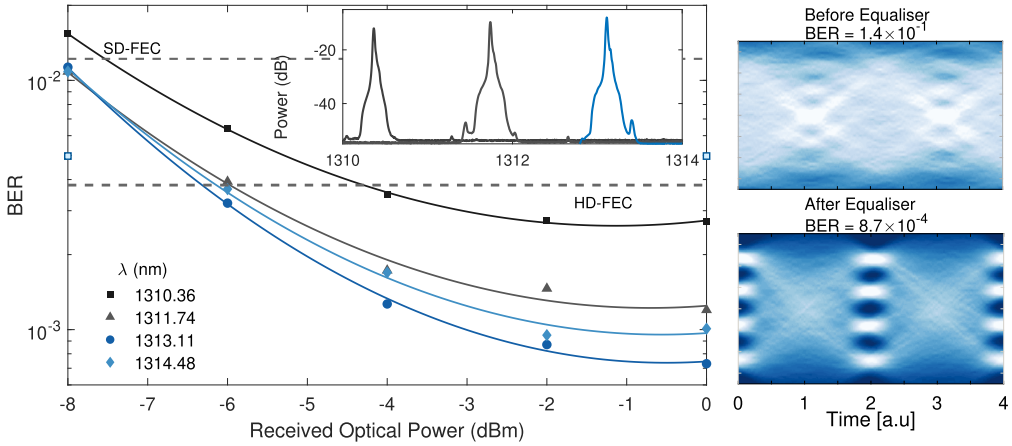

Fig. 11. (Left) BER performance of 50 GBd PAM4 signals after 10 km SMF as a function of received optical power for selected lines, and filtered lines are shown in the inset. (Right) Eye diagram and BER of the filtered wavelength channel (1313.11 nm) at -2 dBm ROP before and after equaliser.

In short-reach systems, especially DCIs, components are expected to operate reliably at elevated ambient temperatures. We now demonstrate the performance of 50 GBd PAM4 signals

Optics EXPRESS

at elevated temperatures of 45°C and 60°C. For this demonstration, we employ a 200 Gsa/S AWG and 256 Gsa/s RTS for the generation and digitisation of the RF signals. The QD-MLL was operated at two different temperatures, and the spectrum redshifts with an increase in temperature as expected. The generated PAM4 signal is modulated using a 30 GHz modulator (MZM1), transmitted in a back-to-back configuration. The test channels at 1325.69 nm for 45°C and at 1339.03 nm for 60°C were filtered using an OBPF and pre-amplified using the quantum well SOA. The signal was then appropriately attenuated using the VOA before detection using a 30 GHz PD. Figure 12 shows the BER performance as a function of ROP for the two test channels (the filtered channel spectrum is shown inset), and the performance falls within the HD-FEC limit for the optical powers received >-6 dBm. Figure 12 inset shows the eye diagram of the signal transmitted at the wavelength of 1325.69 nm and processed at a received optical power of -6 dBm with FFE. These results demonstrate the potential of the QD-MLL to operate effectively at elevated temperatures, making it suitable for DCI applications. We also note that the shift in wavelength with temperature is something that needs to be considered for complete system design.

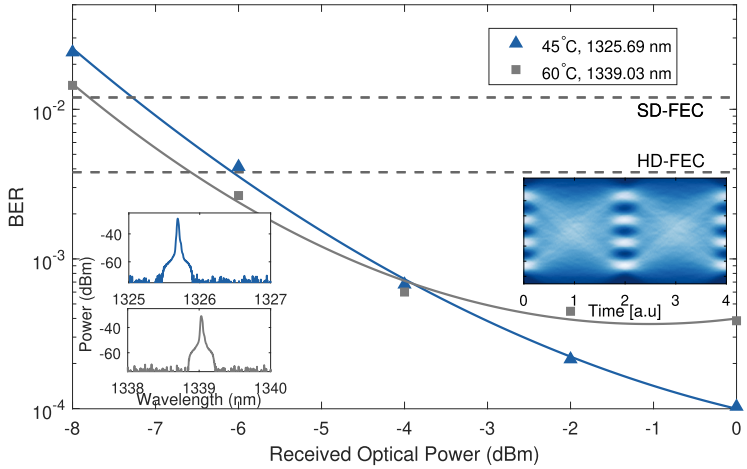

Fig. 12. BER performance of 50 GBd PAM4 as a function of received optical power for selected lines at two different higher temperatures. Insets- (left-top) spectrum of the filtered test channel at 45°C, (left-bottom) spectrum of the filtered test channel at 60°C, and (right) eye diagram of 50 GBd PAM4 signal (1325.69 nm) at -6 dBm ROP.

4. QD-MLL WDM transmission with booster SOA

4.1. Experimental setup for 4×128 GBd OOK transmission

We further demonstrate the capacity enhancement of QD-MLL, performing comb line selection using an optical processor to increase the free spectral range of the comb to support a larger symbol rate per channel. Four alternate lines of QD-MLL were first filtered using a programmable optical processor (waveshaper WSS, 4000B), as shown in Fig. 13. The reconfigured comb line spacing is 160 GHz. The OOK signal is pulse-shaped using an RRC prototype filter with a 0.1 roll-off factor, and 256 GSamples/s AWG (70 GHz bandwidth) generates the continuous-time electrical signal. We then modulate a 128 GBd on-off keyed signal over the four selected lines using the optical modulator (MZM2 with 50 GHz 3-dB bandwidth). The total power of the modulated WDM signal is -9 dBm. We amplify this WDM signal using a single quantum-dot SOA to compensate for the losses from the optical processor and modulator. The amplifier is driven with a 700 mA bias current and operated at 45°C to appropriately align the SOA gain

Optics EXPRESS

curve to the WDM channels. Figure. 16(b) in the Appendix shows the QD-SOA gain and output power as a function of the input power. At the receiver, the amplified WDM signal was processed using a tunable OBPF with an appropriate passband to filter the channel of interest. The 10% port of the 90/10 coupler monitors the optical spectrum using an OSA. The filtered channel in the 90% port is appropriately attenuated using a VOA and detected using a 70 GHz photodiode (XPDV3320R). A 67 GHz bandwidth RF amplifier (SHF M804C) amplifies the detected signal and is then digitised using a 256 GSamples/s RTS (70 GHz bandwidth).

4.2. Results and discussion

We now evaluate the performance of the 128 Gbps OOK signal modulated over four lines of QD-MLL and separated by 160 GHz as shown in Fig. 14(a). The optical spectrum of the modulated WDM signals at the input of QD-SOA and the amplified signal at the output of QD-SOA is shown in Fig. 14(a). A fixed 10 dB attenuator was connected to the OSA to prevent any damage. The spectrum observed at the output of the QD-SOA did not show any artefact of four-wave mixing. Since QD-SOAs offer reduced effects of cross-gain modulation thanks to the high saturation power, employing them for simultaneous amplification of WDM channels in booster configuration is advantageous [27]. Fig. 14 (b) shows the overlapped spectrum of the filtered channels before detecting them at the receiver. As mentioned in the previous subsection, the receiver-side digital signal processing was applied to the digitised samples with a 31-tap FFE. Fig. 15 shows the BER performance as a function of the received optical power for selected line indices, and the performance falls within the HD-FEC limit for the optical powers received >-4 dBm. Figure 15 top-right inset shows two filtered channels, and their modulated-signal to noise power ratio (MSNR) of 22 dB and 25 dB for the lower and longer wavelengths, respectively. The performance of the signals in longer wavelengths is better than that in the first two channels because of the better MSNR of these channels. The relatively higher SNR is suspected to come from better modulation in these channels arising from the optimum polarisation alignment of these channels with the modulator. Figure 15 inset shows the eye diagrams of the four channels evaluated at the received optical power of -3 dBm. The obtained BER values are well below the HD-FEC threshold of 3.8×10^{-3} with 7% overhead, indicating the potential of arbitrarily low bit error upon applying forward error correction.

We now evaluate the energy consumption of the components (QD-MLL optical frequency comb and the SOAs) used in the WDM transmission experiments. Table 1 shows the measured electrical energy consumption of the QD-MLL, the SOA preamplifier and the booster SOA used in the high-capacity data transmission experiments. The values are calculated from the drive current and its corresponding measured voltage for the operation of each device. We note here that the modulator/driver and receiver will be the other main elements contributing to the link's overall energy consumption, and the value remains unchanged regardless of the type of source laser and amplifiers. Detailed energy analysis of the modulators is presented in [7,17]. We can observe that using a single booster SOA for WDM systems reduces the power consumption in terms of pJ/bit compared to the case where an SOA is used for each wavelength channel. By increasing the number of wavelength channels amplified by a single SOA, the energy consumption per bit can be further reduced. For the energy consumption of the MLL, preamplifier (each for every 100 Gbps per channel) and booster amplifier, we have assumed a total rate of 1, 1, and 0.512 Terabit/s, respectively.

Optics EXPRESS

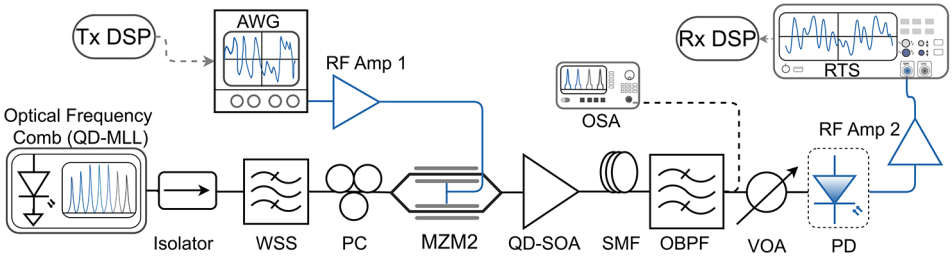

Fig. 13. Schematic of the experimental setup for the data transmission with four channel 128 Gbps OOK signal and employing a single QD-SOA booster amplifier.

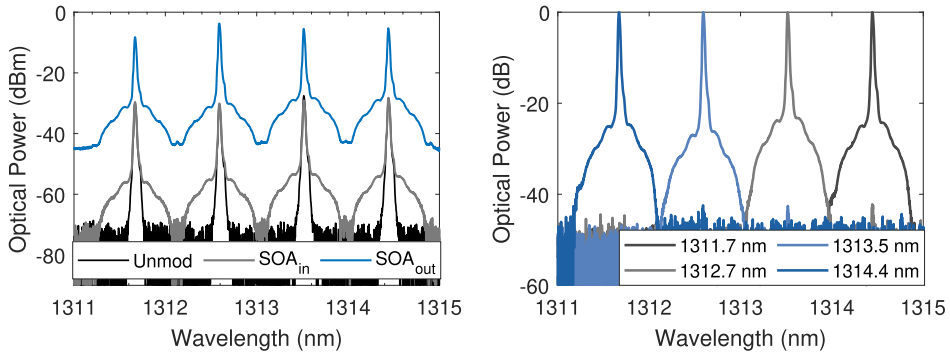

Fig. 14. (a) Optical spectrum of the unmodulated filtered comb lines, modulated signals at the input of SOA and the amplified signal at the output of SOA. (b) Filtered 128 GBd OOK signals before detection.

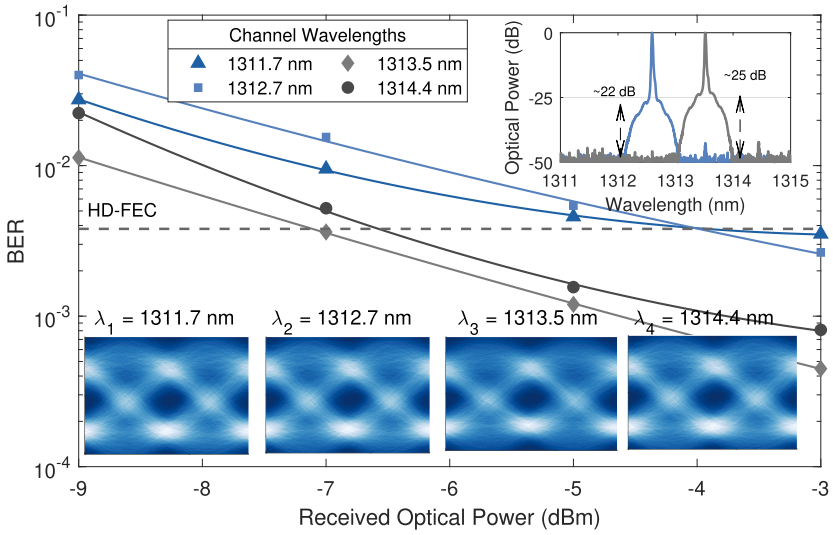

Fig. 15. BER performance of 128 GBd OOK signals as a function of received optical power. The inset shows the eye diagram of the four channels at -3 dBm ROP. The top-right inset shows the filtered two channels along with the estimate of modulated-signal-to-noise ratio.

Optics EXPRESS

Table 1. Energy consumption of considered subsystems

	Power	No. of devices	Energy/bit
QD-MLL	284.2 mW	1	284.2 fJ/bit
SOA Preamplifier	180 mW	10	1.8 pJ/bit
Booster SOA	924 mW	1	1.8 pJ/bit

5. Conclusions

Increasing data transport capacity in the campus DCI links has become necessary due to the wide use of cloud-based applications. With photonic integration and wide wavelength tuning capability, the single chip GaAs-based quantum dot-based laser comb could be deployed for next-generation multi-lane transmission systems. This work demonstrated a total data rate of 1.4 Tbps and 1 Tbps over 10 km SMF with 100 Gbps/λ PAM4 and PS-PAM8 signals employing the QD-MLL source and an SOA preamplifier for each channel, with performance being within the standard FEC limits. We have also demonstrated 128 Gbps/λ OOK optical transport using the QD-MLL and a single SOA to amplify all channels, enabling energy-efficient high-speed transmission within DCs. System performance can be optimised by increasing the carrier power before modulation or employing SOAs with a wider dynamic range and reduced nonlinear distortions [27,28]. In addition, the use of nonlinear equalisers and advanced signal processing algorithms can improve the performance of higher-order PAM signals in the presence of SOA nonlinearity [29]. Using a single booster SOA for simultaneous amplification of multiple wavelengths can greatly reduce the system's overall power consumption while also helping achieve optimum system performance. Due to the target DCI applications, the demonstrations presented here were limited to IM/DD systems. However the lower phase noise characteristics of the QD-MLL would also enable ultra-high capacity phase modulated lightwave transmission. The device can potentially enable the next generation of 800 GbE and 1.6 TbE energy-efficient links through photonic integration with suitable modulators and amplifiers for IM/DD and coherent short-reach systems.

Appendix

The total gain and output power as a function of the input power for the quantum-well and quantum-dor SOAs are shown in Fig. 16(a) and 16(b), respectively. The QW-SOA was operated at 150 mA bias current and at 21°C temperature. The gain curve is measured for an operating wavelength of 1310 nm. The bandwidth of this SOA is about 70 nm, having a uniform gain

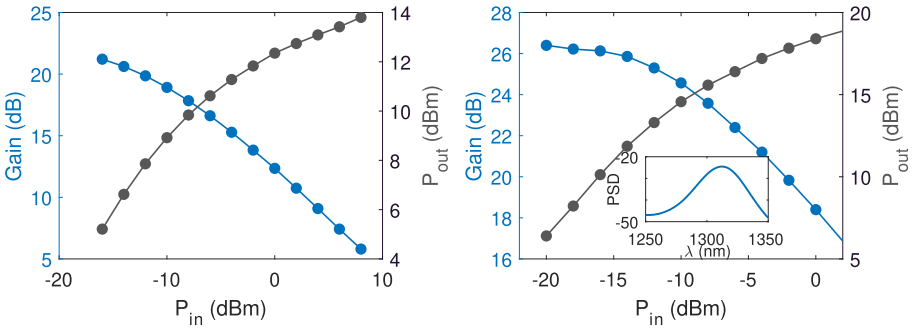

Fig. 16. SOA gain and output power as a function of the input power for (a) Quantum-well SOA and (b) Quantum-dot SOA.

Optics EXPRESS

across the QD-MLL lines. On the other hand, the QD-SOA was operated at 700 mA, and the temperature was tuned to 45°C to have a uniform gain across the selected lines of operation. The ASE spectrum of the OSA at these operating conditions is shown as an inset in Fig. 16(b). The gain curve was measured for a continuous wave signal at 1312.98 nm.

Funding. Science Foundation Ireland (13/RC/2077 P2, 12/RC/2276 P2, 23/IRDIFB/11955); HORIZON EUROPE European Innovation Council (101136762 (UNICO), 101137000 (M-Engine)); Irish Research eLibrary.

Acknowledgment. The authors would like to acknowledge colleagues in IEO for useful guidance and constructive conversations. Open access funding provided by Irish Research eLibrary. The authors also acknowledge Coherent, Inc. for lending the O-band optical processor (Waveshaper 4000B) for measurements.

Disclosures. The authors declare no conflicts of interest.

Data Availability. Data underlying the results presented in this paper are not publicly available at this time but may be obtained from the authors upon reasonable request.

References

1. C. Xie and B. Zhang, "Scaling optical interconnects for hyperscale data center networks," Proc. IEEE **110**(11), 1699–1713 (2022).
2. S. Pan, H. Zhang, Z. Liu, *et al.*, "Multi-wavelength 128 Gbit $s^{-1}\lambda^{-1}$ PAM4 optical transmission enabled by a 100 GHz quantum dot mode-locked optical frequency comb," J. Phys. D: Appl. Phys. **55**(14), 144001 (2022).
3. X. Zhou and H. Liu, "Short range optical transmission for emerging 5G, DCI and Metro Networks," ECOC **W3**, (2016).
4. M. Dumont, S. Liu, M. Kennedy, *et al.*, "High-efficiency quantum dot lasers as comb sources for DWDM applications," Appl. Sci. **12**(4), 1836 (2022).
5. L. N. Venkatasubramani, H. Xu, M. Buyalo, *et al.*, "100 Gbps/λ transmission with quantum dot O-Band comb source using 50 GBd PAM4/16QAM-OFDM signals," in *2023 Optical Fiber Communications Conference and Exhibition (OFC)*, (IEEE, 2023), pp.1–3.
6. A. Netherton, M. Dumont, Z. Nelson, *et al.*, "25.1 Short-Reach Silicon Photonic Interconnects with Quantum Dot Mode Locked Laser Comb Sources," in *2024 IEEE International Solid-State Circuits Conference (ISSCC)*, vol. 67, (IEEE, 2024), pp.422–424.
7. J. Chen, B. Yang, J. Qin, *et al.*, "Energy efficient and high bandwidth quantum dot comb laser based silicon microring transmitter for optical interconnects," IEEE J. Sel. Top. Quantum Electron. **31**, 1–10 (2025).
8. S. Bernal, M. Dumont, E. Berikaa, *et al.*, "12.1 terabit/second data center interconnects using O-band coherent transmission with QD-MLL frequency combs," Nat. Commun. **15**(1), 7741 (2024).
9. J. Rautert, M. S. Buyalo, V. Mikhrin, *et al.*, "Ultra-wideband, flat-top, 100 ghz spacing quantum-dot comb laser for cw-wdm data transmission in o-band," in *2025 Optical Fiber Communications Conference and Exhibition (OFC)*, (IEEE, 2025), pp.1–3.
10. N. Taengnoi, K. R. Bottrill, N. K. Thipparapu, *et al.*, "WDM transmission with in-line amplification at 1.3 μm using a Bi-doped fiber amplifier," J. Lightwave Technol. **37**(8), 1826–1830 (2019).
11. A. Sobhanan, A. Anthur, S. O'Duill, *et al.*, "Semiconductor optical amplifiers: recent advances and applications," Adv. Opt. Photonics **14**(3), 571–651 (2022).
12. L. N. Venkatasubramani, A. G. Reza, and L. Barry, "On the application of semiconductor optical amplifier towards Terabit/s short-reach IM/DD transmission systems," in *Next-Generation Optical Communication: Components, Sub-Systems, and Systems XIII*, vol. 12894 (SPIE, 2024), pp.70–73.
13. L. N. Venkatasubramani, A. G. Reza, A. R. Gautam, *et al.*, "Tbps IM/DD transmission over 10 km SMF with O-band quantum dot laser comb for DCIs," in *2024 Optical Fiber Communications Conference and Exhibition (OFC)*, (IEEE, 2024), pp.1–3.
14. J. Tang, "The Shannon channel capacity of dispersion-free nonlinear optical fiber transmission," J. Lightwave Technol. **19**(8), 1104–1109 (2001).
15. D. Kong, H. Xin, K. Kim, *et al.*, "300 Gb/s net-rate intra-datacenter interconnects with a silicon integrated optical frequency comb modulator," in *2020 Optical Fiber Communications Conference And Exhibition (OFC)*, (IEEE, 2020), pp.1–3.
16. Y. Yuan, Y. Peng, W. V. Sorin, *et al.*, "A 5× 200 Gbps microring modulator silicon chip empowered by two-segment Z-shape junctions," Nat. Commun. **15**(1), 918 (2024).
17. H. Cai, Z. Liao, Y. Zhang, *et al.*, "Microcomb and micro-ring modulator driven DWDM optical transmitter with ultra-high speed of 20 × 128 Gb/s," J. Lightwave Technol. **43**(15), 1–17 (2025).
18. C. Shang, Y. Wan, J. Selvidge, *et al.*, "Perspectives on advances in quantum dot lasers and integration with Si photonic integrated circuits," ACS Photonics **8**(9), 2555–2566 (2021).
19. C. Shang, K. Feng, E. T. Hughes, *et al.*, "Electrically pumped quantum-dot lasers grown on 300 mm patterned Si photonic wafers," Light:Sci. Appl. **11**(1), 299 (2022).
20. M. Buyalo, A. Gubenko, S. Mikhrin, *et al.*, "Efficient, high-power, narrow-linewidth, continuous-wave quantum-dot semiconductor comb laser," Sci. Rep. **14**(1), 4197 (2024).

Optics EXPRESS

21. G. Morthier and P. Vankwikelberge, *Handbook of distributed feedback laser diodes*, (Artech House, 2013.
22. S. P. Ó. Dúill and L. P. Barry, "Simplified laser frequency noise measurement using the delayed self-heterodyne method," Photonics **11**(9), 813 (2024).
23. K. Kikuchi, "Characterization of semiconductor-laser phase noise and estimation of bit-error rate performance with low-speed offline digital coherent receivers," Opt. Express **20**(5), 5291–5302 (2012).
24. F. Kärtner, *Few-Cycle Laser Pulse Generation and Its Applications* Topics in Applied Physics (Springer, 2004).
25. A. G. Reza, M. T. Costas, C. Browning, *et al.*, "124.8-Gbit/s net data rate capacity for IM/DD optical intra-data center interconnections by utilizing probabilistically shaped PAM-8 and digital linear feed-forward equalizers," in *2022 Asia Communications and Photonics Conference (ACP)*, (IEEE, 2022), pp.997–1000.
26. ITU-T, "International Telecommunication Union (ITU-T) G.709.2/ Y.1331.2 recommendation," (07/2018).
27. A. G. Reza, L. N. Venkatasubramani, A. R. Gautam, *et al.*, "2× 53 Gbit/s PAM-4 transmission using 1.3 μm DML with high power budget enabled by quantum-dot SOA," IEEE Photonics Technol. Lett. **37**(1), 1–4 (2025).
28. L. N. Venkatasubramani, A. G. Reza, V. S. Mikhrin, *et al.*, "100 Gbps PAM4 transmissions over 50 km with 40 dB power budget for PON using a high-gain quantum dot SOA," in *2024 Optical Fiber Communication Conference*, (Optica Publishing Group, 2024), pp.1–3.
29. K. Wang, C. Wang, J. Zhang, *et al.*, "Mitigation of SOA-induced nonlinearity with the aid of deep learning neural networks," J. Lightwave Technol. **40**(4), 979–986 (2022).